Theoretical
and Applied
Climatology

[1] Division of Meteorology-Climatology, Department of Geology, Aristotle University of Thessaloniki,
  Thessaloniki, Greece
[2] Department of Geography, University of the Aegean, Mytilene, Greece
[3] NASA/Goddard Space Flight Center, Laboratory for Atmospheres, Greenbelt, USA
[4] Science Systems and Applications Inc., Lanham, Maryland, USA
[5] Foundation for Research and Technology – HELLAS, Regional Analysis Division,
  Institute of Applied and Computational Mathematics, Heraklion, Crete, Greece

Validation of an infrared-based satellite algorithm to estimate accumulated rainfall over the Mediterranean basin

H. Feidas[1], G. Kokolatos[2], A. Negri[3], M. Manyin[4], N. Chrysoulakis[5], Y. Kamarianakis[5]

With 7 Figures

Summary

The potential of an infrared-based satellite rainfall algo-
rithm, the well-known Convective-Stratiform technique
(CST), to estimate accumulated rainfall in the Mediterra-
nean basin is tested. The CST, calibrated by coincident,
physically retrieved rainfall rates from the Tropical Rainfall
Measuring Mission (TRMM) Precipitation Radar (PR), is
applied over the central-eastern Mediterranean region for
the twelve-month period September 2004–August 2005.
Estimates from this technique are verified over a $1° \times 1°$
gridded precipitation dataset, based on rain gauge data only,
for different time scales (monthly, seasonal and annual).
The comparisons between satellite-derived precipitation
estimates and validation data provide a high correla-
tion coefficient (0.88) and low biases only for the summer
season. In contrast, the comparison statistics for winter
demonstrate the shortcomings of the CST algorithm in
reproducing adequately the precipitation field in the mid-
latitudes during this season. Although the correlations for
spring and annual precipitation are relatively high (0.76 and
0.73, respectively), a strong positive bias exists. Rainfall
variability is less adequately reproduced for the autumn, but

the errors are within an acceptable range. A comparison test
conducted in the different climate zones of the study area
indicated that the calibrated CST performs better in the sub-
tropical deserts and steppes of northern Africa and in
humid, continental climates. Mediterranean climates pro-
duce higher correlations for autumn, summer and spring
precipitation, whereas humid sub-tropical climates present
the lowest correlation coefficients. Finally, the potential of
the CST technique in climatic studies was demonstrated by
studying the diurnal variability of precipitation at high
spatial and temporal resolutions.

1. Introduction

Ground-based techniques such as those using
rain gauges and radars suffer from spatial and/or
temporal coverage problems. Conventional rain-
gauge networks provide relatively accurate
measurements at specific points, but their use is
restricted by the high spatial and temporal vari-
ability of rainfall. The limited sampling area of
rain gauges and especially their uneven distribu-
tion constitute a substantial problem when deal-
ing with effective spatial coverage. In addition,
remote and uninhabited areas are not covered by

Correspondence: Haralambos Feidas, Division of Meteorology-
Climatology, Department of Geology, Aristotle University of
Thessaloniki, Thessaloniki 54124, Greece, e-mail: xfeidas@geo.
aegean.gr

conventional observation networks. Similar problems are associated with the use of weather radars. Ground-based radar systems provide fairly continuous spatial and temporal coverage, but the conversion from reflectivity to rainfall rate relies on many assumptions. Moreover, the quantitative range of radar measurements is generally limited to 150 km or less. Most importantly, both rain gauges and radars provide incomplete coverage, particularly over the sea, where such instruments are virtually non-existent. As a consequence of ground observations from gauge and radar suffering from spatial and temporal discontinuities, rainfall estimates derived by meteorological satellites became an attractive alternative due to their high sampling frequencies in space and time. Satellite-based rainfall estimates provide full spatial coverage and often offer the only near real-time (15–30 minutes) precipitation estimates in many areas. Moreover, only instruments onboard satellite platforms are able to make rainfall estimates over remote areas of land or water where data are difficult or impossible to collect from the ground. Consequently, satellite rainfall monitoring has been used widely to address the key issues of continuous spatial and temporal coverage, which cannot be achieved by other observing systems. There are two primary means of measuring rainfall from satellite-based sensors: thermal infrared and passive microwave techniques.

When infrared (IR) satellite data first became available, precipitation was correlated to the cloud-top temperature with the use of empirical relationships. Numerous new precipitation estimation algorithms that use infrared data as the only data input have been developed; e.g., the Arkin technique (Arkin 1979), the Area Time Integral (ATI) technique (Doneaud et al. 1984; Lopez et al. 1989), the GOES Precipitation Index (GPI) (Arkin and Meisner 1987), the Griffith-Woodley Technique (GWT) (Griffith et al. 1976, 1978, 1981), Negri-Adler-Woodley Technique (NAWT) (Negri et al. 1984), the Convective-Stratiform Technique (CST) (Adler and Negri 1988) and the technique for Precipitation Estimation from Remotely Sensed Information using Artificial Neural Networks (PERSIANN) (Hsu et al. 1997; Hong et al. 2004). From a physical point of view, the relationship between cloud-top temperature and surface rainfall rate is very indirect when infrared techniques are used to estimate rainfall. In contrast, microwave measurements from passive sensors aboard low Earth-orbiting satellites provide more direct and physical connections between the upwelling microwave radiation and hydrometeors. However, the problem with passive microwave rainfall rates is that they are extremely sparse in space and time. Passive microwave sensors have a narrowed spatial coverage and are located only on polar-orbiting satellites, which pass any particular location on the Earth's surface twice a day at most. This time interval between two successive microwave measurements is much too large to account for the high spatial and temporal variability of rainfall. It is therefore unlikely that a user requiring a current estimate of rainfall over a particular region could obtain a timely passive microwave rainfall rate. Consequently, the accumulated rainfall computed by time integration of instantaneous estimated rainfall rates are derived with very large uncertainties.

In contrast, infrared geostationary instruments have the advantage of high temporal resolution. As a result of very good data sampling, and despite the fact that infrared measurements have no direct physical connection with surface precipitation, infrared techniques provide reliable estimates of accumulated rainfall amounts over long time periods, and averaged over large areas. These techniques are most appropriate for large and climatic scales. GPI is one of the commonly used and archived infrared techniques for climatological studies (Arkin and Meisner 1987; Arkin and Janowiak 1991). The Third Algorithm Intercomparison Project shows that the infrared method scores higher than the microwave method for monthly mean rainfall estimation (Ebert and Manton 1998). This result is due mostly to the higher temporal sampling of the infrared dataset.

Visible (VIS) channels are generally used as supplemental information to screen out cold clouds, which are optically thin and potentially non-precipitating, from optically thick and, therefore, likely precipitating clouds. The role, however, of visible data in improving infrared rainfall estimates is significant only in the case of warm rainfall. Results from the First Algorithm Intercomparison Project (AIP/1) over Japan (King et al. 1995) showed a higher correlation with validation data using bispectral meth-

ods (IR/VIS) over the infrared-based techniques alone for the case of warm, orographically induced rainfall. For cold, bright clouds the correlations were similar. The main problem, however, with visible imagery is that it is only usable during the time that the sun angle is high. As a result, the performance of the related bispectral methods is more likely to be a strong function of the time of day and, therefore, more likely to introduce erroneously day-night biases in precipitation estimates. The latter point is the reason why bispectral methods are seldom used for the retrieval of rainfall parameters (especially on climatic scales), and that most of the rainfall algorithms rely solely upon infrared data.

Most infrared-based techniques for rainfall estimation have been developed and tested for the study of precipitation systems in specific areas and provide precipitation estimates that change as a function of the particular region. Thus, traditional infrared-based techniques fail to provide rainfall estimates that can be used globally, for all seasons of the year, and for a variety of weather regimes. Rainfall characteristics vary according to different climate regimes, consequently, any infrared method must be adapted to the geoclimatic conditions of the region of interest, and validated against appropriate in situ measurements taken over the study area before any application is made. Such investigations have been made for Greece by Feidas (2006) and Feidas et al. (2006), for the Iberian Peninsula by Tarruella and Jorge (2003), for Sardinia by Marrocu et al. (1993), for the Korean peninsula by Oh et al. (2002) and for Eastern Africa by Menz (1997).

The Convective-Stratiform Technique (CST) is a satellite infrared technique designed to estimate precipitation at the scale of individual thunderstorms. The original technique (Adler and Negri 1988) was developed for application over southern Florida, and was calibrated by output from a 1-D model. The CST method is complex and is related to the general geoclimatic conditions for which it was originally developed. The modifications to adapt it to different climates and different meteorological situations require appropriate validation and calibration campaigns of measurements to be organized and carried out on the target area. According to a recent study of Feidas (2006), the CST could provide the best

overall performance in measuring rainfall, provided that the method is adjusted to the geoclimatic conditions of Greece. With the launch of the Tropical Rainfall Measuring Mission (TRMM) in November 1997, high quality, high resolution, instantaneous microwave-based estimates became available from the (passive) TRMM Microwave Radiometer (TMI) and the (active) TRMM Precipitation Radar (PR). Negri et al. (2002, 2003) used TMI and PR derived rainfall rates to recalibrate the CST over northern South America and the globe, respectively, and then applied the recalibrated technique to the study of diurnal rainfall variability. A similar approach was followed by Feidas et al. (2006) to recalibrate the CST for the Mediterranean region using coincident, physically retrieved rainfall rates from the TRMM PR, and then evaluate its performance in the study of rainfall events of different intensity over the region.

The lack of conventional observation networks over sea and mountainous zones, and the lack of ground radars over the eastern Mediterranean to monitor rainfall, makes the use of satellite imagery essential in representing the spatial distribution of precipitation with a high spatial resolution and geographic coverage. In the present study, the CST is validated over the central-eastern Mediterranean region in order to test its performance in estimating accumulated rainfall using Meteosat-7 satellite data. In addition, the possibility of its application for climatic analysis is also examined. The long-term archive of Meteosat-7 images make this dataset appropriate for this kind of climatic study. Emphasis is given to the potential of the technique in studying the diurnal variability of precipitation at high spatial and temporal resolutions. CST was chosen because, until this time, it is the only infrared-based technique that has not yet been validated for large and climatic scales in the mid-latitudes. It has only been applied for forecasting in the Mediterranean basin, but here we try to apply it for climatic purposes. Comparing CST with the other IR-based techniques, CST is a more sophisticated technique that utilizes distributions of both cloud brightness temperature and texture features. The validation of CST in the Mediterranean region will increase our knowledge regarding the potential use of infrared-based techniques for estimating rainfall in mid-latitudes. Given that

CST, as for many of the other IR-based techniques, was originally developed and tested for the study of tropical convective systems, we used the recalibrated version of the technique developed by Feidas et al. (2006).

2. Datasets

The data used in this study comprises infrared data from the Meteosat-7 satellite, and a gridded dataset based on rain gauge observations for a twelve-month period (September 2004–August 2005).

2.1 Satellite observations

Meteosat-7 satellite images covering the Mediterranean basin were available at half-hourly intervals for the period of interest. The infrared Meteosat images used in this study cover the spectral range of 10.5–12.5 μm with a spatial resolution at the satellite sub-point of $5 \times 5\,km^2$ and $5.6 \times 7\,km^2$ over the eastern Mediterranean. Images have been preprocessed in EUMETSAT (European Organisation for the Exploitation of Meteorological Satellites). The satellite data were recorded in counts from 0 to 255. The corresponding radiances were obtained from EUMETSAT's calibration data and converted into brightness temperatures through a lookup table. A simple linear interpolation process was used to obtain the exact brightness temperature corresponding to the measured radiances.

2.2 Gauge observations

The precipitation data produced by the Global Precipitation Climatology Centre (GPCC) (http://gpcc.dwd.de), based on rain gauge data only, were used to verify the precipitation estimates and evaluate the precipitation maps obtained by the CST method. The products of the GPCC, gauge-based gridded precipitation datasets, are used by international researchers, e.g., within water-related projects of the World Meteorological Organization (WMO), United Nations Educational, Scientific and Cultural Organization (UNESCO), Food and Agriculture Organization (FAO), and the United Nations Environment Programme (UNEP), in order to provide a reliable and robust basis for the analysis of spatial precipitation structures. Verification of monthly satellite-based precipitation estimates is one of the main applications of the GPCC dataset (e.g., Janowiak 1992; Xie and Arkin 1995; Kaestner 2003; Tarruella and Jorge 2003; Kaestner et al. 2006). The bias corrected version of the GPCC gauge-based Monitoring Product is used as the land-surface reference for the GPCP (Global Precipitation Climatology project) satellite-gauge combined product, which is available at a resolution of 2.5° lat/long.

The GPCC creates global gridded precipitation datasets using quality-controlled data from 7000 in situ gauge observations. This dataset, termed Monitoring Product, provides monthly area-mean precipitation totals (mm/month) on a $1° \times 1°$ grid box template for the period 1986 to present. The available area-mean data are useful for budget studies and are comparable to satellite-based estimates or model results on corresponding grids. The calculation of area means on the grid cells from gauge observations consists of three major steps (Rudolf and Schneider 2005):

(1) Irregularly distributed gauge observations are interpolated onto a regular grid with a mesh size of 0.5°lat/long using an adapted version of the empirical interpolation method SPHEREMAP (Willmott et al. 1985). SPHEREMAP is a spherical adaptation of the Shepard (1968) empirical weighting scheme, which takes into account (a) the distance of the stations to the grid point (for a limited number of the nearest stations), (b) the directional distribution of stations versus the grid point (in order to avoid the overweighting of clustered stations), and (c) the gradients of the data field in the grid point environment. SPHEREMAP was selected, adapted and implemented at GPCC in 1991 for the operational objective analysis of global precipitation, following external studies (Legates 1987; Bussieres and Hogg 1989) and internal intercomparison results (Rudolf et al. 1992, 1994).

(2) Area-averaged precipitation is first calculated as an arithmetic mean from the interpolated data of (up to) 4 grid points representing the corners of a 0.5° grid cell. Only those grid points are used which are located over land, so the mean represents land-surface precipitation.

(3) Area-mean precipitation on a coarser grid (1°
or 2.5°) is then calculated as a weighted av-
erage of the corresponding 0.5° grid cells
where each 0.5° grid cell used has the weight
of its land-surface proportion within the total
grid cell.

The two most critical errors in the gridded data-
set of GPCC are the systematic gauge measuring
error and the sampling error. The systematic
gauge measuring error generally leads to an
undercatch, particularly for solid precipitation
and during high wind speeds (Goodison et al.
1998). The gridded gauge-analysis products pro-
vided by the GPCC are not bias corrected for
systematic gauge measuring errors. However,
the GPCC provides estimates for that error, using
the Legates (1987) climatological correction fac-
tors. The dataset used in this study was corrected
for systematic errors using the correction factors
recommended by the GPCC.

The sampling error of area-mean precipita-
tion calculated from point data depends on the
gridding process, the number of stations, and
the regional variability of the precipitation field
according to the climatic/orographic conditions
(WMO 1985). GPCC provides data with the num-
ber of gauges used per grid cell for the individual
month. Due to the complex gridding process
used, the final product includes grid cells corre-
sponding to zero number of stations; those grid
cells were excluded from the dataset used in the
present study. Given that grid cells with more
than two gauges are clustered and account only
for 22% of the dataset sample in the study area,
we used all grid cells with a number of gauges
greater than one in order to ensure spatial unifor-
mity of the data, as well as the required density
for the comparison analysis applied in the climat-
ic zones of the Mediterranean basin.

Finally, rainfall rates recorded by a network of
34 stations distributed evenly over Greece were
used to verify the diurnal cycle of precipitation
retrieved by the CST algorithm.

3. The calibrated CST algorithm

In its original form, the CST method was devel-
oped and tested in order to study convective pre-
cipitation systems in the tropical Atlantic and
mid- and low-latitude continental areas (Adler
and Negri 1988). Since IR techniques, such as

CST, can only estimate precipitation indirectly,
the estimated values are technique-dependent.
Moreover, the retrieval techniques change as a
function of the particular region. As a result, cal-
ibration of the CST parameters to the geoclimatic
conditions of the area of interest is usually re-
quired before any application is made.

In the present study, we used the version of
the CST that has been recalibrated over the
Mediterranean basin by Feidas et al. (2006) using
coincident rainfall estimates from the TRMM PR
for the wet period of a hydrological year (2003–
2004). More than 1000 TRMM orbits distributed
evenly throughout the Mediterranean basin were
used for the calibration. The goal of the recali-
bration was to determine parameters so that the
CST will be able to reproduce the total rain vol-
ume and the PR-observed division between con-
vective and stratiform rain for the Mediterranean
region using infrared data from the Meteosat-7
satellite. The CST was adjusted on a statistical
basis, over the calibration period, without explic-
it constraints on instantaneous rainfall estimates.
The recalibrated technique, termed CST/Met-7,
is applied in five steps:

(1) The method locates, in an array of infrared
data, all local brightness temperature minima
(T_{min}) in the IR Meteosat-7 images with
$T_{min} < 253$ K.
(2) The deviation of each T_{min} from the back-
ground temperature (slope), defined as the
average temperature of the eight surrounding
pixels, is computed.
(3) The point of a local minimum T_{min} is as-
sumed to be a convective centre using a
probability function that determines the
probability of convective rainfall for a given
T_{min} and slope value. This procedure, defined
as the slope test, was introduced to eliminate
the minima originated by thin cirrus clouds,
which are non-precipitating clouds.
(4) Rainfall rate and rainfall area are assigned to
each minimum point, which has passed the
slope test, as a function of its T_{min}, based on
the PR calibration parameters.
(5) A stratiform rain area is then identified around
each convective centre for those cloud pixels
colder than a brightness temperature thresh-
old, which have not already been assigned rain
of convective origin. A constant lower rainfall
rate is assigned to all the pixels in this area.

4. Validation of the CST algorithm

4.1 Comparison methodology

The most obvious constraint in directly comparing measurements from rain gauges to satellite derived precipitation estimates is that gauges give point measurements while satellites produce spatial averages. It is always problematic to compare a rainfall amount collected in a small opening to a satellite estimate averaged over a large area. Moreover, only gridded analyses of precipitation can be used to validate the spatial variability of the satellite-based precipitation estimates. Therefore, the comparison of the CST/Met-7 precipitation estimates with observations from rain gauges was made in terms of area-mean precipitation totals.

First, monthly, seasonal and annual pixel-based precipitation totals were calculated from half-hourly Meteosat-7 IR measurements, for a twelve-month period (September 2004–August 2005). More than 17,500 images have been analysed in this study. Then, rain gauge precipitation averaged over a $1° \times 1°$ grid box (GPCC dataset) was compared to average regional satellite precipitation. Monthly area-mean precipitation totals (mm/month) of the gridded GPCC data were used as validation data, whereas the corresponding average regional satellite precipitation was defined as the arithmetic average value of rainfall totals estimated by the algorithm for each pixel

in a grid cell. The study area covers the central-eastern Mediterranean region extending from $29°$ N to $47°$ N, and $9°$ E to $37°$ E, and comprises 465 GPCC grid cells (Fig. 1). Meteosat-7 zenith viewing angles may vary from $33°$ to $56°$ in this area. According to Joyce et al. (2001), the previous range of zenith angle values may introduce errors in the brightness temperatures that vary from less than $3°$ to almost $6°$. This means that the spatial variability of the bias related to the limb darkening effect is less than $4°$, a value that was not considered as an important contributing error factor in the precipitation estimates.

For each comparison, several measures of the closeness of the estimates to the observed values were calculated, such as the correlation coefficient (r), the root mean square difference (RMSD), the bias, the mean absolute difference (MAD) and the percent difference (PD). These are defined as follows:

$$\text{RMSD} = \sqrt{\left(\frac{1}{n}\sum_{i=1}^{n}(S_i - G_i)^2\right)},$$

$$\text{Bias} = \frac{1}{n}\sum_{i=1}^{n}(S_i - G_i)$$

$$\text{MAD} = \frac{1}{n}\sum_{i=1}^{n}|S_i - G_i|,$$

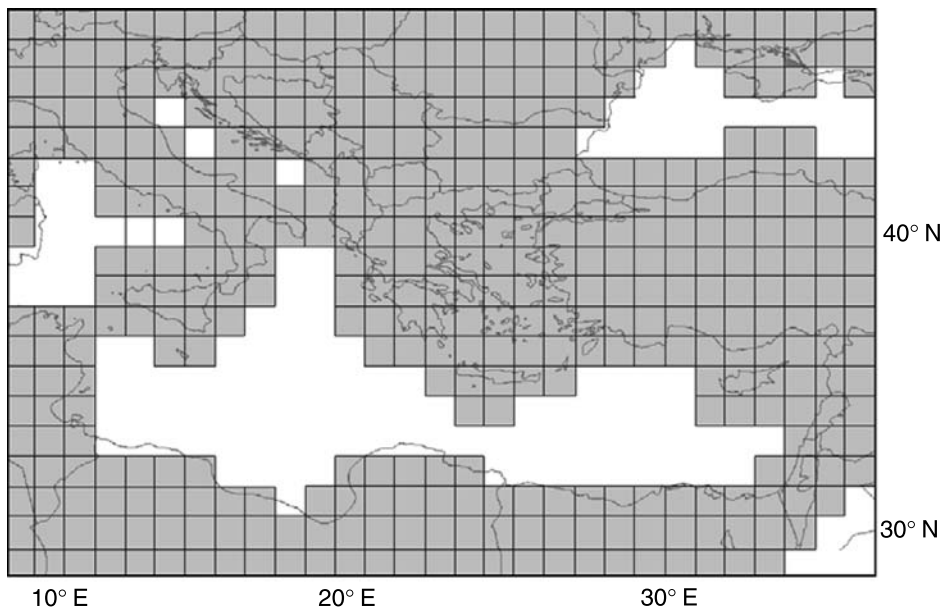$$\text{PD} = \frac{1}{n}\sum_{i=1}^{n}\frac{|S_i - G_i|}{G_i} \tag{1}$$

Fig. 1. The GPCC grid box template in the area of study
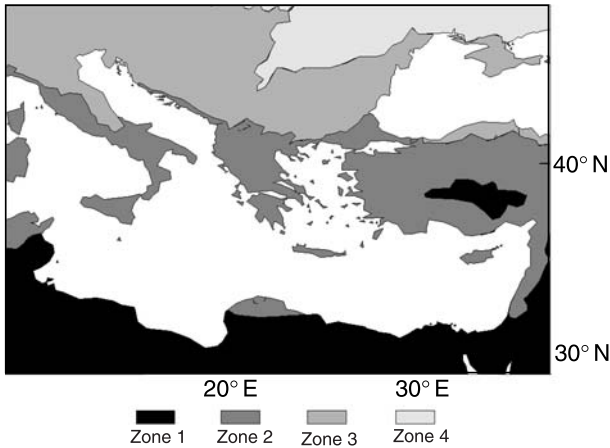
Fig. 2. The four climatic zones in the area of study. Zone 1: Subtropical and midlatitude deserts and steppes, Zone 2: mediterranean climates, Zone 3: humid subtropical climates, Zone 4: humid continental climates

where S_i is the estimated value and G_i is the validation value.

To examine CST performance over the different climatic zones of the Mediterranean basin, the previous comparison methodology was also implemented to each of the major regional climates in the study area. According to the Köppen climate classification system (Köppen and Geiger 1936), the area of study belongs to regional climates B (arid climates), C (mild mid-latitude), D (severe mid-latitude), and H (highlands), which are further divided into sub-categories. For the requirements of this paper, the study area was divided into four different zones (Fig. 2):

- Zone 1. Sub-tropical and mid-latitude deserts and steppes, which correspond to the sub-category with codes BWh, BSh and BSk (arid, dry sub-tropical climates).
- Zone 2. Mediterranean climates, which correspond to the sub-categories with codes Csa, and Csb (mild mid-latitude climates with dry, hot or warm summers).
- Zone 3. Humid sub-tropical climates, which correspond to the sub-category with code Cfa (humid, temperate climates with mild winters, no distinct dry season and warm summers).
- Zone 4. Humid continental climates, which correspond to the sub-category with the code Dfa (humid mid-latitudes with severe winter, no dry season cold climates and warm summers).

The highland climate of the Alps was intergrated into Zone 3 since it constitutes a small region in the area of study, covering a small number of GPCC grid boxes.

4.2 Comparison results

We determined the agreement between the average regional precipitation measured by rain gauges in a $1° \times 1°$ grid box (GPCC data) with the corresponding average estimated from the calibrated CST algorithm, according to the methodology described in the previous paragraph. The comparison was made in terms of precipitation totals estimated in monthly, seasonal and annual intervals for the period September 2004–August 2005.

Scatter diagrams for seasonal, annual and two representative monthly totals (January and July) are presented in Fig. 3 with the associated statistics provided in Table 1. This type of comparison resulted in a range of rather moderate to high correlation coefficients (0.48–0.90) for all months with the exception of January and February whose correlation coefficients have very low values (0.28 and 0.32, respectively). Given that the highest correlation is obtained for the period March to October (*r* values from 0.61 to 0.90), it was concluded that rainfall variability could be reproduced adequately by the CST for this period of the year. The deviation between satellite estimates and validation data can be evaluated by assessing the estimation errors. The high positive values of bias errors in winter and spring months indicate a systematic overestimation of the precipitation values. This overestimation is decreased substantially for autumn months and turns to a slight underestimation for the summer, with differences smaller than 35% of the gauge values. The remaining estimation errors present a similar pattern with larger errors obtained for the period January to May, smallest errors during summer, and acceptable errors for autumn. The reason for the large values of PD statistics for April, May and June is that very small rainfall amounts were recorded by several rain gauges. The modified CST algorithm presents a different phase in the interannual precipitation cycle with maxima in January and April, compared to the maximum of November found in the observations. This shift in the phase
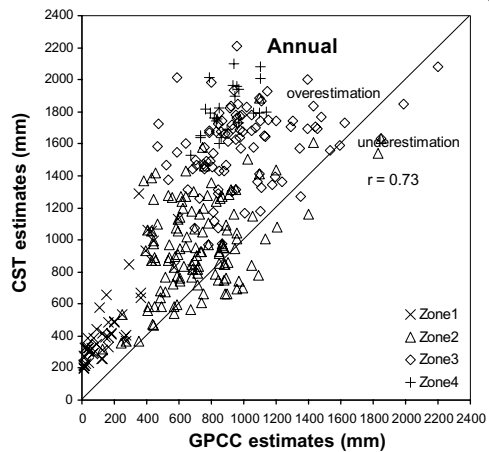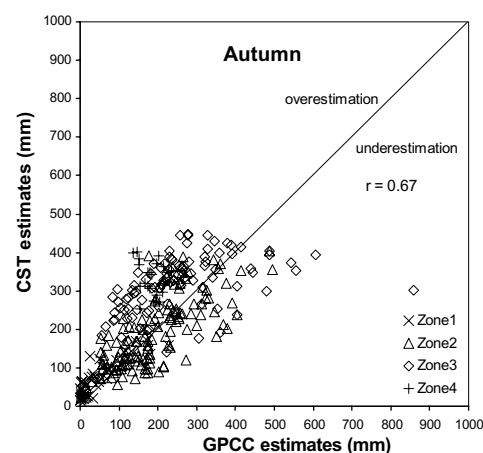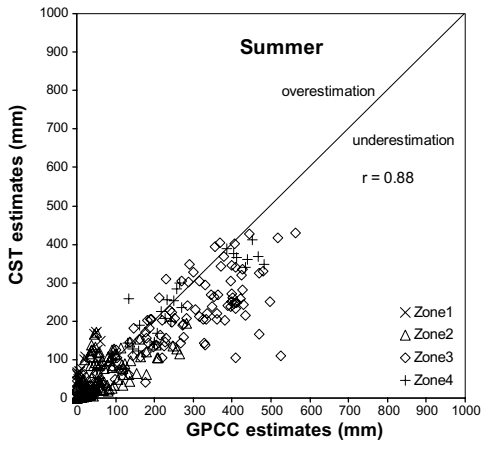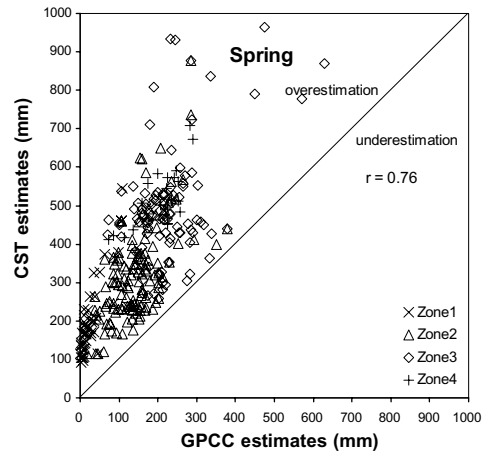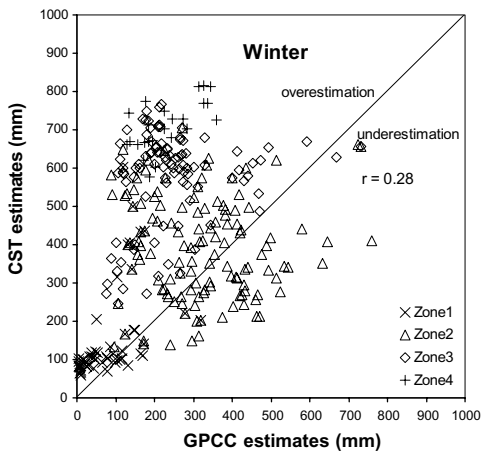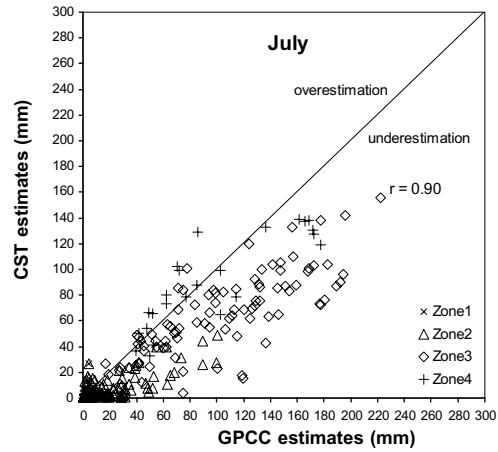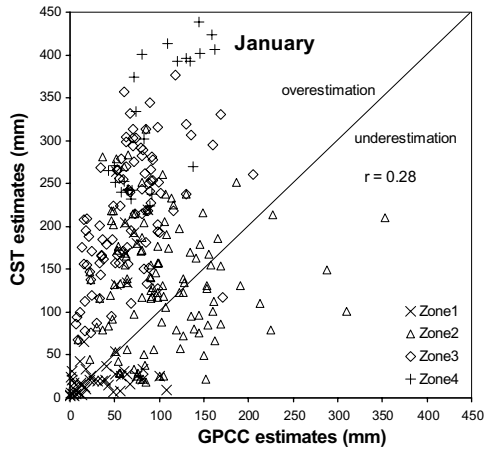
Table 1. Comparison statistics of CST/Met-7 accumulated rain retrievals for all temporal scales considering GPCC monthly area-mean precipitation totals on a $1° \times 1°$ grid box template (273–280 grid cells) (period September 2004–August 2005)

Period	Mean (mm)		Median (mm)		Bias (mm)	MAD (mm)	RMSD (mm)	PD	r
	GPCC	CST	GPCC	CST					
September	37.8	31.0	37.2	32.0	−6.9	14.4	28.0	1.4	0.67
October	52.2	66.9	34.5	69.2	14.7	32.3	45.2	4.8	0.65
November	99.5	128.8	91.1	121.4	29.1	57.1	71.6	1.8	0.48
December	87.4	125.1	70.4	129.5	37.6	57.3	69.7	2.5	0.49
January	79.6	162.7	71.7	157.3	83.1	105.7	131.5	2.4	0.28
February	81.7	157.8	72.1	154.4	76.0	95.7	119.9	2.0	0.32
March	57.2	124.6	46.5	116.5	67.4	69.8	85.0	2.3	0.70
April	53.6	164.6	47.7	164.1	111.0	111.3	125.0	56.0	0.61
May	47.2	88.6	43.5	89.0	41.4	44.2	55.4	26.8	0.73
June	42.3	47.9	30.7	46.2	5.6	21.5	32.4	18.7	0.65
July	50.0	31.8	27.9	10.3	−18.2	20.9	33.2	0.9	0.90
August	59.9	44.1	27.0	25.6	−15.8	22.1	37.9	0.6	0.88
Autumn	188.4	225.5	176.2	234.2	37.1	80.1	107.1	1.3	0.67
Winter	247.4	443.5	226.5	460.3	196.2	237.2	293.4	1.7	0.28
Spring	158.5	379.3	158.9	362.5	220.8	220.8	249.8	3.7	0.76
Summer	153.2	124.2	91.1	101.8	−29.1	53.9	82.3	7.4	0.88
Annual	747.5	1172.5	766.7	1218.4	425.0	458.2	556.0	1.4	0.73

of the interannual cycle is the result of the high positive bias induced by the CST algorithm for the period January to April. According to the previous results, rainfall variability is best represented with acceptable estimation errors only for the period June to October.

The previous findings are in agreement with the comparison statistics for the seasonal precipitation totals. The higher correlation obtained for the summer and spring seasons ($r = 0.88$ and 0.76, respectively) suggests that the CST technique may provide the best overall performance in reproducing the spatial distribution of accumulated precipitation in the Mediterranean for these two seasons. The high estimation errors, however, for spring may constitute a restriction in their use for quantitative estimations for this season. A comparison of the median with mean values indicates an influence of some extreme events on the low summer rainfall, which is well captured by the CST technique. The method's performance in estimating autumn precipitation totals is satisfactory with a moderate correlation coefficient (0.67) and relatively acceptable errors (differences at about 20% of the gauge values). The CST/Met-

7 method is not able to reproduce adequately the spatial distribution of winter precipitation ($r = 0.28$) even though precipitation estimates are area averaged over $1° \times 1°$ grid cells. Finally, accumulated annual precipitation satellite estimates are well correlated ($r = 0.73$) with the validation data, as a result of the relatively good correlation found for the three seasons: summer, autumn and spring (r ranging from 0.67 to 0.90). Nevertheless, there still exists a significant precipitation overestimation and, in general, error values are relatively high (differences of 57% of the gauge values) as a result of the contribution of the high positive bias of the winter and spring precipitation in a large part of the study area.

The previous findings are also reflected in the pattern of the scatter diagrams in Fig. 3. The scatter diagram for summer precipitation exhibits the best performance compared to the other seasons, with a more evenly distributed pattern, which is in agreement with its highest correlation coefficient (0.88). The points lying along the Y-axis indicate that the CST/Met-7 method classifies some low-level rain pixels as positive even

Fig. 3. Scatter diagrams of GPCC estimates and CST/Met-7 retrieved rain totals averaged on a $1° \times 1°$ grid cell for seasonal, annual and two monthly intervals (period September 2004–August 2005). Points representing precipitation totals in the four climatic zones of the study area are indicated with different symbols

if there is no trace of rain in the gauge measurements. The distribution of points in the scatter diagrams becomes more uneven and widespread towards winter with evident indications of over-estimation of precipitation totals. In particular, the pattern of the diagram becomes more widespread from summer to autumn when the first indications of overestimation are revealed. Even though spring precipitation totals are very well correlated with gauge values, a significant over-estimation is evident throughout the entire dataset. The poor correlation for winter precipitation results in the uneven and widespread distribution

of points in the respective scatter diagram. An inspection of the corresponding scatter diagrams in Fig. 3 shows that the overestimation of the spring and annual precipitation totals increases significantly with increasing accumulated precipitation. The poor performance of the technique for winter rainfall could be attributed to a systematic overestimation of precipitation in a part of the study area (see the bulk in the upper-left part of the scatter diagram) related to climatic Zones 3 and 4, which is evident when considering the contribution of each climatic zone to the scatter diagram for winter. These scatter

Table 2. Correlation coefficients, bias, RMSD, mean and median obtained from the comparison of the CST/Met-7 seasonal and annual accumulated rain retrievals with the GPCC dataset, considering the four climatic zones in the study area. Corresponding statistics for the whole area are also given for comparison

	Whole area	Zone 1	Zone 2	Zone 3	Zone 4
(a) Correlation coefficients					
Autumn	0.67	0.90	0.74	0.47	0.09
Winter	0.28	0.50	0.13	0.23	0.64
Spring	0.76	0.84	0.61	0.47	0.74
Summer	0.88	0.71	0.63	0.73	0.90
Annual	0.73	0.85	0.48	0.35	0.54
(b) Bias					
Autumn	37.1	24.6	−1.7	62.7	145.5
Winter	196.2	74.7	69.5	331.6	478.7
Spring	220.8	178.6	181.0	262.1	310.1
Summer	−29.1	25.1	−6.5	−78.2	−23.3
Annual	425.0	302.9	242.3	578.3	910.9
(c) RMSD					
Autumn	107.1	36.2	69.2	132.2	155.6
Winter	293.4	131.4	205.0	364.4	482.1
Spring	249.8	194.7	207.1	294.8	314.6
Summer	82.3	42.7	48.1	114.4	57.3
Annual	556.0	342.1	379.5	672.0	921.2

	Whole area		Zone 1		Zone 2		Zone 3		Zone 4	
	GPCC	CST	GPCC	CST	GPCC	CST	GPCC	CST	GPCC	CST
(d) Mean										
Autumn	188.4	225.5	51.8	76.4	195.6	193.9	253.8	316.6	186.1	331.6
Winter	247.4	443.5	84.1	158.9	322.5	392.0	246.0	577.5	230.8	709.5
Spring	158.5	379.3	35.1	213.7	142.1	323.1	226.0	488.1	202.7	512.8
Summer	153.2	124.2	9.8	34.9	63.5	57.0	290.8	212.6	282.3	259.0
Annual	747.5	1172.5	180.9	483.8	723.6	965.9	1016.6	1594.8	902.0	1812.9
(e) Median										
Autumn	176.2	234.2	28.1	64.5	179.5	181.2	232.9	326.8	186.5	332.4
Winter	226.5	460.3	76.7	106.3	313.8	397.2	223.9	606.9	214.4	708.1
Spring	158.9	362.5	17.2	179.5	137.4	301.5	214.6	464.6	222.4	503.4
Summer	91.1	101.8	0.9	21.0	46.3	41.4	290.3	206.0	246.2	255.0
Annual	766.7	1218.4	129.6	387.9	619.9	943.2	949.6	1646.6	878.9	1793.2

diagrams demonstrate how the high positive bias introduced by the CST in winter and spring precipitation estimates contributes into the strong overestimation in the annual precipitation estimates. The scatter diagrams of the two representative months (January and July) demonstrate exactly the same pattern with the season they belong to (winter and summer, respectively).

Table 2 shows the correlation coefficients, the bias and the root mean square difference (RMSD) obtained from the comparison of the CST/Met-7 seasonal and annual accumulated rain retrievals with the GPCC dataset, considering the four climatic zones in the study area. Mean and median values for both datasets are also given in the table. The contribution of each climatic zone to the distribution of points in the scatter diagrams of Fig. 3 is shown through points with different symbols.

A first inspection of the results reveals that the CST/Met-7 performs better in the sub-tropical deserts and steppes of northern Africa (Zone 1) and in humid continental climates (Zone 4). The high correlation for Zone 1 throughout the year (0.50 for winter, and from 0.71 to 0.90 for the other seasons) could be due to the dominant rainfall pattern in this area. Most precipitation in these regions is of convective origin, and is localized and of short duration. The CST technique was specifically devised to detect such convective precipitation. In addition, mean rainfall in Zone 1 is lower than that in other climatic zones and this probably contributes to the best fit found for this area. With regard to the median values, it seems that the low mean rainfall in Zone 1 is influenced by some extreme events. Zone 4 (humid continental climates) gives a very high correlation for the summer (0.90), and high correlations for winter and spring precipitation (0.64 and 0.74, respectively). Zone 2 (Mediterranean climates) presents the highest correlations in autumn, summer and spring (from 0.61 to 0.74). Zone 3 (humid sub-tropical climates) provides the lowest correlation coefficients with the exception of summer precipitation which is reproduced adequately by CST ($r = 0.73$). As expected, summer precipitation is reproduced adequately in all climatic zones with correlation coefficients ranging from 0.63 to 0.90. Note that mean summer rainfall in Zones 3 and 4 is not only high but is also the highest during the year.

According to the median values, only summer precipitation in Zones 2 and 4 might be influenced by extreme events. The poor correlation in Zones 2 and 3 for winter precipitation could be due to the thick middle and high cloud layers, with possible orographic enhancement effects and frontal situations, associated with the cyclonic activity which characterizes the winter weather conditions in these regions. Infrared-based techniques are deficient in detecting rainfall in such cloud systems even if their parameters are adjusted to the conditions of the study area. Considering estimation errors, Zones 1 and 2 present the smallest bias and RMSD, whereas errors for Zone 3, and especially Zone 4, are quite large. These last two zones (3 and 4) contribute most to the poor performance of the CST technique in reproducing winter precipitation over the whole study area. Relative errors, however, increase substantially for Zone 1 when mean precipitation is taken into account, as a result of the very low precipitation recorded by rain gauges in this area.

Next, the calibrated CST algorithm is validated qualitatively in order to examine whether the spatial distribution of precipitation totals could be accurately determined. Figure 4 shows the maps of seasonal and annual accumulated precipitation obtained from the application of the CST/Met-7 and the GPCC map. For comparison with the GPCC map, the estimations of the technique were averaged for a $1° \times 1°$ grid cell resolution. The map produced for summer using the CST technique is the most similar to the GPCC map, in agreement with the best comparison statistics found for this season among the others. Locations and magnitudes of local precipitation maxima in the CST precipitation field coincide adequately with those of the rain gauge network. Even though precipitation distribution for spring is also reproduced very well, a significant overestimation of rainfall is evident across the study area, which is in agreement with the high estimation errors found in the validation analysis. The CST/Met-7 technique exhibits a spatial rainfall distribution for autumn which is in general agreement with the rainfall pattern obtained using the rain gauge network. However, precipitation is overestimated in some places in the Balkans and northern Italy, resulting in poor correlations and large biases for climatic Zones 3 and 4 (see Table 2). The comparison of both maps for win-
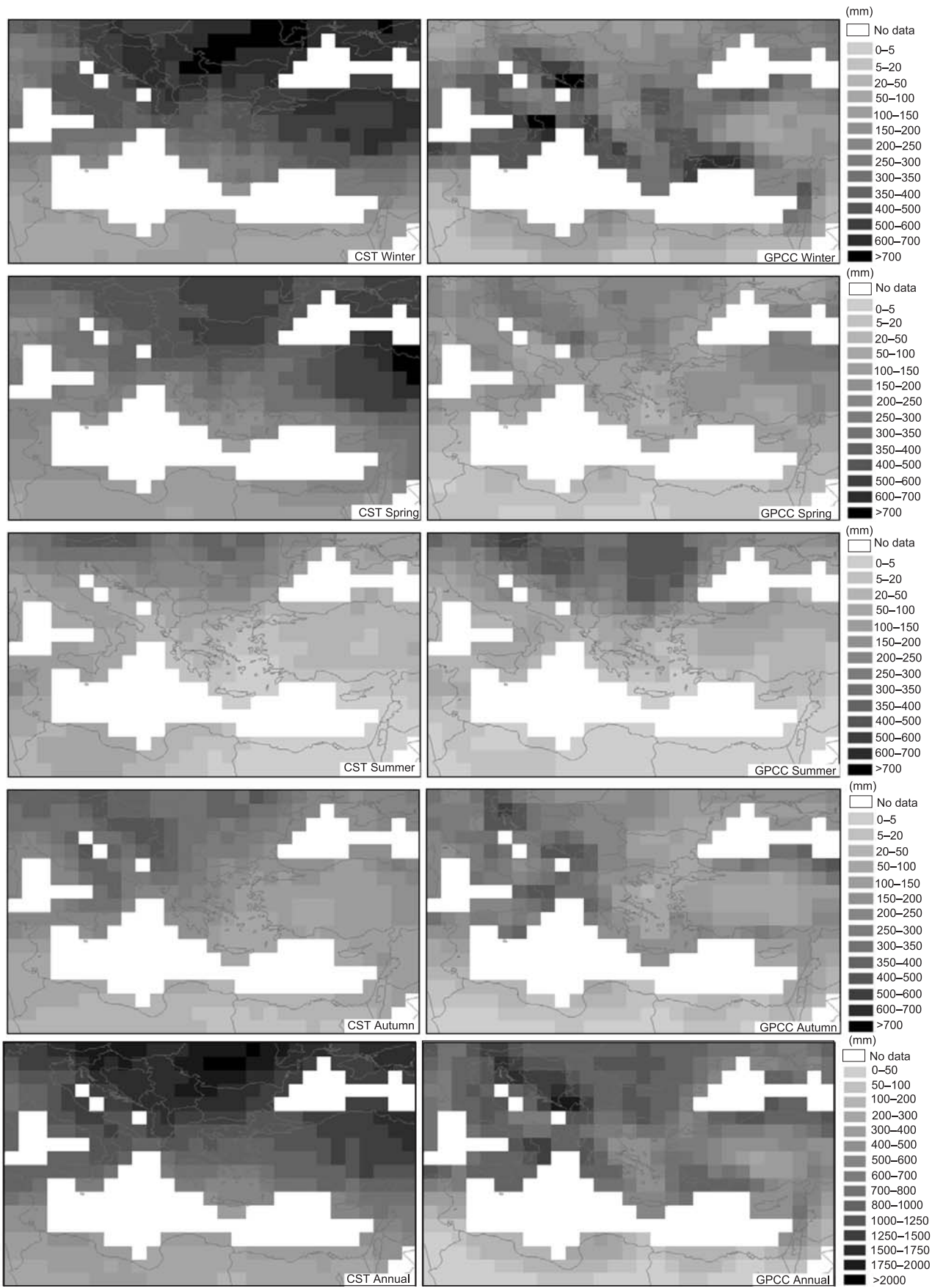
Fig. 4. Precipitation maps of seasonal and annual precipitation totals averaged on a $1° \times 1°$ grid cell and elaborated using calibrated CST and GPCC estimates (period September 2004–August 2005)

ter demonstrates the shortcomings of the CST algorithm in reproducing adequately the precipitation field during this season, mainly in the inner
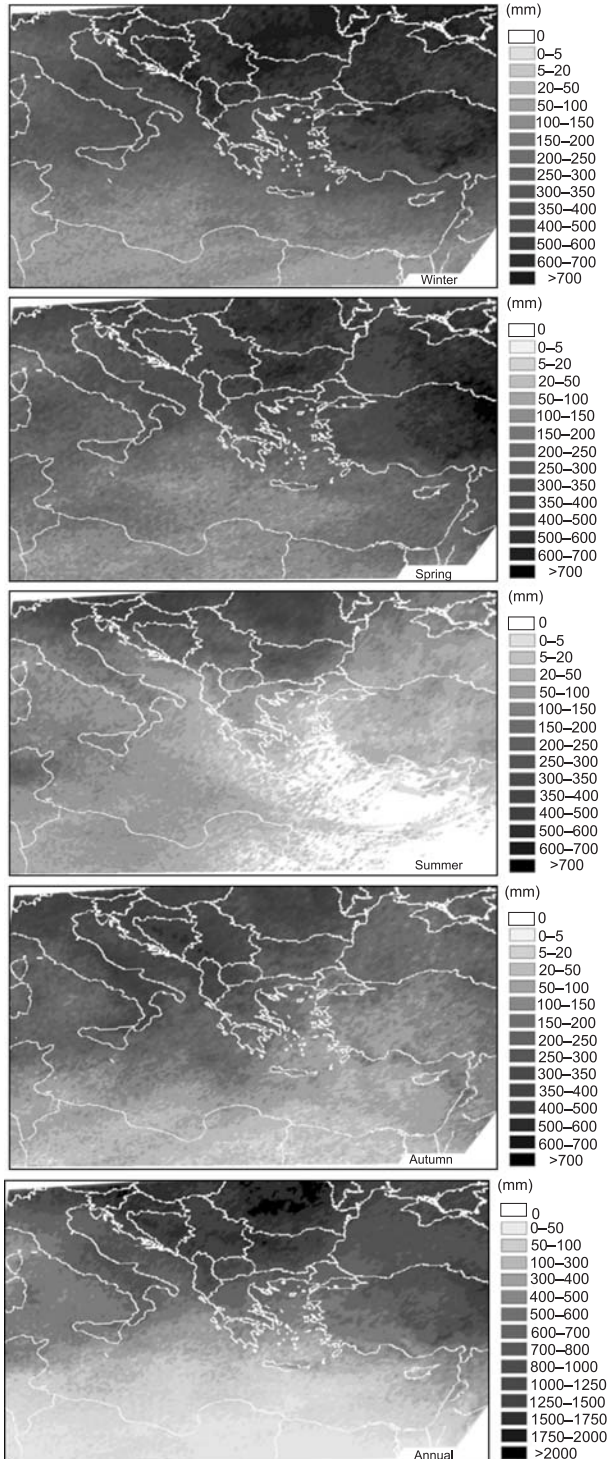

Fig. 5. Precipitation maps of seasonal and annual precipitation totals on a Meteosat projection elaborated using calibrated CST (period September 2004–August 2005)

continental areas of Turkey (part of Zone 2) and the Balkans (Zones 3 and 4, and part of Zone 2). Finally, the satellite technique provides a more adequate reproduction of the spatial variability of annual precipitation ($r = 0.73$) but a strong overestimation of precipitation is evident in many places, mainly in climatic Zones 1 and 4.

The advantages of using satellite derived precipitation maps are revealed in Fig. 5 where maps of seasonal and annual accumulated precipitation obtained from the calibrated CST algorithm using the full spatial resolution of Meteosat-7 ($5.6 \times 7 \, \text{km}^2$ at the area of interest) are presented. We are not able to examine the accuracy of these high resolution maps but the information extracted from these maps during the warm season – when the CST/Met-7 performs best – would be useful. These rainfall maps show a greater spatial resolution than the GPCC map. Moreover, they can estimate the rainfall over the sea and remote areas and illustrate descriptively the effect of orography on the distribution of precipitation. This is clearly depicted in autumn where most of the rainfall along the main mountain ranges in the area is of orographic origin.

The most important finding is the very good performance of the CST/Met-7 method in estimating accumulated rainfall at monthly and seasonal intervals for the warm season. This was expected since the synoptic situation during the warm season in the Mediterranean basin is characterized by stable weather conditions and a lack of cyclonic activity due to the extension of the Azores anticyclone into central Europe and the Mediterranean region. As a result, May to September constitutes the dry period of the year when most precipitation originates from convective activity triggered by thermal instability over land. The CST technique was specifically designed to detect such convective rainfall. In contrast, the thick middle and high cloud layers associated with the fronts passing over the Mediterranean region from November to March are considered as precipitating clouds by the CST method, even though there is no precipitation. In these cases, the CST detects too many temperature minima that are not screened efficiently by the method and, consequently, they are erroneously assumed to be centres of convective rainfall.

5. Diurnal cycle

The main goal of this study was to investigate the potential of the CST technique in estimating accumulated precipitation over the Mediterranean basin for climatic purposes. One of the most important advantages of infrared-based techniques for estimating precipitation – such as CST – is the high temporal sampling of data produced by the high temporal resolution of geostationary satellites (15–30 min). This feature allows the extraction of the diurnal cycle of precipitation with high spatial and temporal resolution. Following the success of the CST/Met-7 technique on the warm season of the Mediterranean region, we attempted to investigate the potential of the technique in reproducing the diurnal variability of precipitation at a high temporal resolution. We chose to examine the period May–August 2005, given that a diurnal cycle of rainfall is more likely during these months due to the absence of significant synoptic weather systems over the area. This situation allows the development of favourable thermal instability over land, due to daytime heating that triggers convective activity in the afternoon.

To examine the potential of the CST in estimating the diurnal variability of precipitation in Greece, we made estimates of the mean rainfall rate at 30 min intervals in a region encompassing the Greek Peninsula (see the inset in the panel of Fig. 6). Validation data from 34 rain gauges, distributed evenly over Greece, were used to verify the diurnal cycle derived by the CST estimates
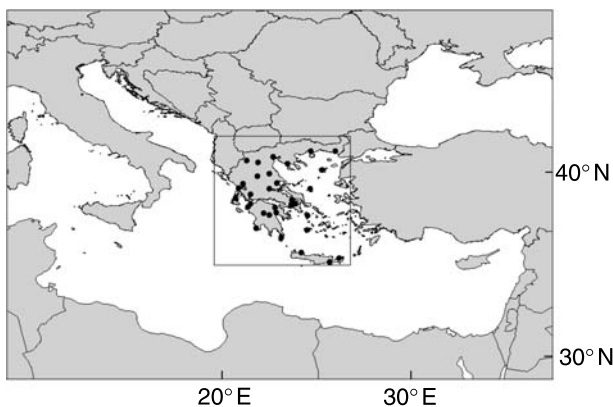

Fig. 6. Locations of rain gauge network used as ground truth data in Greece. The inset frame delineates the area used for the study of the diurnal cycle of precipitation in Greek Peninsula

(Fig. 6). The rain gauge network comprises inland as well as coastal stations. In order to validate the CST technique in representing the diurnal cycle of precipitation, the diurnal variation of three rainfall parameters was computed over Greece at 30 min intervals during the period May–August 2005, using gauge data and satellite estimates. These parameters are:

a. the *mean rainfall rate*, partitioned by convective and stratiform components,
b. the *convective rainfall fraction* defined as the percentage of measured rainfall volume due to convective rainfall, and
c. the *convective rainfall area fraction* defined as the percentage of the rainfall area classified as convective.

Satellite estimates were made using 3×3 Meteosat pixels, centred over the pixel corresponding to each station; thus a total of 306 pixels (34 stations $\times$ 9 pixels) per Meteosat image were used to calculate the three rainfall parameters. This was done to reduce the effect of the error arising from the uncertainty of ± 1 pixel in the co-location of the rain gauge stations on the Meteosat images. The rainfall parameters that require information on the convective component were computed based on the CST/Met-7 convective-stratiform rain division. In the case of rain gauges, the same rainfall parameters were estimated using a rainfall rate threshold of 6 mm/h. Mean rainfall rates recorded at 30 min intervals by rain gauges were considered convective with a value equal to or above that threshold, bearing in mind that there is not a standard rainfall rate threshold to distinguish the two types of rainfall. This simple criterion has been employed by many researchers, with thresholds ranging from 5 to 10 mm/h (e.g., Atlas et al. 2002; Nzeukou et al. 2002; Schumacher and Houze 2003; Tenório and Kwon 2006). We chose the threshold of 6 mm/h in order to make the convective rainfall parameters derived by both satellite estimates and rain gauge data comparable, since this is the lowest convective rainfall rate assigned by the CST/Met-7.

Figure 7 shows the diurnal variation of the three rainfall parameters computed as discussed earlier during the period of May–August 2005 over Greece. Time series indicate a typical diurnal variation of precipitation with a pronounced
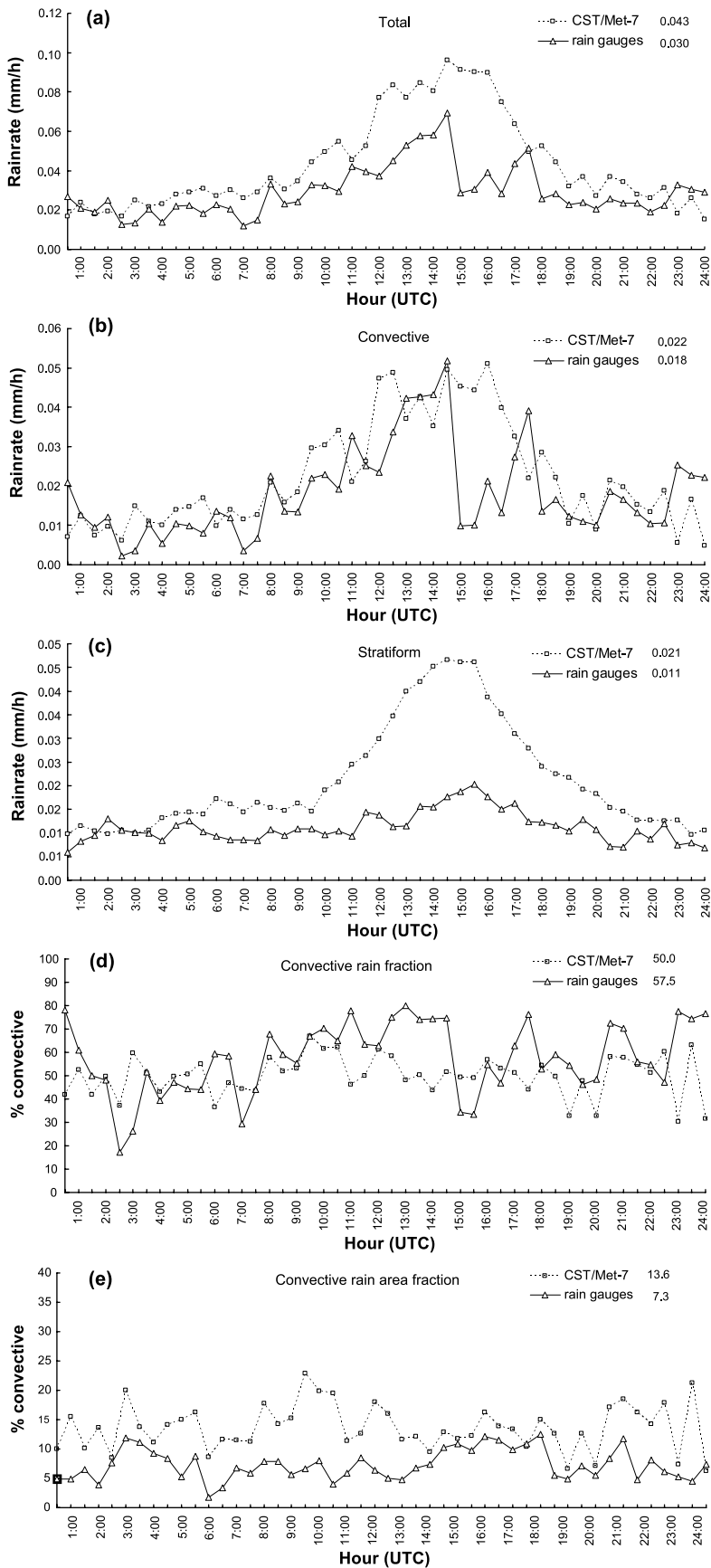
Fig. 7. Diurnal variation of five rain parameters for the CST/Met-7 estimates and rain gauges in the period May–August 2005 over Greece. The mean for each parameter is plotted in the upper right-hand corner of each panel. (**a**) Mean rain rate partitioned into (**b**) convective and (**c**) stratiform components. (**d**) Convective rain fraction. (**e**) Convective rain area fraction

rainfall maximum at between about 1400 and 1600 UTC (1700–1900 local time), no doubt in response to the daytime heating that triggers convective activity in the afternoon. The timing of the diurnal cycle of the satellite estimates for both total rainfall and the division into convective and stratiform components is generally consistent with the analysis of rain gauge data (Fig. 7a–c). The satellite estimates overestimate the gauge rainfall rate, but we are more interested in getting the phase correct than addressing the bias. An interesting finding is that the convective component of the CST/Met-7 rainfall rate (Fig. 7b) is in very good agreement with the rain gauges. Both curves exhibit sharp fluctuations due to the few rain samples. In examining just the stratiform component of the rainfall (Fig. 7c), we find that satellite estimates are higher than the rain gauge data, a fact that accounts for a great part of the overestimation of the total rainfall rate displayed in Fig. 7a.

When examining only the two rainfall parameters related to convective rainfall – convective rainfall fraction and convective rainfall area fraction – we again find a good agreement in the diurnal variation of the two datasets (Fig. 7d, e). This supports the previous finding that CST/Met-7 reproduces efficiently the convective component of precipitation. The satellite estimates reveal that convective rainfall constitutes 14% of the rainfall area while accounting for 50% of the rainfall volume. Similar figures for the rain gauges are 7% and 57%. This comparison suggests that CST/Met-7 overestimates slightly the convective rainfall area but provides an efficient division between convective and stratiform rainfall. The doubling of the CST/Met-7 derived convective rainfall area fraction should be considered with regard to the small magnitude of the values found for this parameter. This overestimation, however, indicates that either the technique locates erroneously a larger number of convective cores, or that the calibration of the CST/Met-7 overestimated the average convective area assigned to each convective core.

6. Conclusions

In this paper we have presented results from a satellite infrared technique, the convective-stratiform technique, for estimating accumulated precipitation over central-eastern Mediterranean using Meteosat-7 satellite data. The parameters of the technique were calibrated to the geoclimatic conditions of the Mediterranean region using coincident, physically retrieved rainfall rates from the PR of TRMM satellite. With the aim of increasing our knowledge of the potential of using infrared-based techniques for estimating rainfall in mid-latitudes, we examined the possibility of its application for climatic purposes.

Verification of the monthly, seasonal and annual CST/Met-7 results for a twelve-month period was performed using the $1° \times 1°$ gridded GPCC dataset in the central-eastern Mediterranean region. When considering the verification results, we reach the following conclusions:

- Summer precipitation is best represented by the CST/Met-7.
- The spatial variability of rainfall is very well represented for spring, but a significant overestimation is produced by the retrieval technique that has to be taken into account before any application is made.
- Rainfall variability is less adequately reproduced for autumn but errors are still acceptable, at least for September and October.
- All statistics – correlation coefficient and estimation errors – indicate that winter precipitation cannot be reproduced adequately by CST/Met-7.
- Even though the correlation of annual precipitation estimates with gauge values is rather high, the strong positive bias introduced by winter and spring precipitation prevents the use of annual totals in quantitative climatic studies with a certain level of accuracy.

According to the previous results, the calibrated CST provides the best overall performance in reproducing the spatial distribution of accumulated precipitation in the Mediterranean region for the warm season of the year, when most precipitation originates from convective activity triggered by thermal instability over land. The CST technique was specifically designed to detect such convective rainfall. On the contrary, the comparison statistics for winter demonstrate the limitations of the CST algorithm in reproducing adequately the precipitation field in mid-latitudes during this season. This is due to the inherent shortcoming of infrared techniques – originally

developed for convective cloud systems over the tropics – in discriminating convection in frontal clouds in the mid-latitudes. It seems that the slope test introduced by CST and the adjustments of the calibrated CST to the geoclimatic conditions of the Mediterranean basin were not adequate in removing cirrus clouds. CST clearly needs improvements, at least for the winter season. The regional adjustments of the CST/Met-7 method need to be improved to be useful beyond an application that is limited by region and by time. With the advent of Meteosat-8, carrying the high spectral resolution SEVIRI (Spinning Enhanced Visible and Infrared Imager) several additional tests based on split-window algorithms could be applied for the screening of cirrus clouds in order to improve the CST performance. A further development of this work could be in this direction. Since these data are available only after 2004, infrared-based techniques, with their ability to extend their coverage back to 1970s, provide unique datasets in the study of rainfall over the last three decades around the globe, and to gain further insights into periodic variations in precipitation amounts and distributions. Moreover, simple infrared-based methods retain a certain level of climatological value since their estimates are incorporated in the new microwave-infrared merged products.

Seasonality is not a feature that characterizes the CST alone. One of the common characteristics of all satellite algorithms (infrared, microwave etc) is that they perform best in the warm season (convective rainfall), and worst during winter. This is one of the results of the International Precipitation Working Group (IPWG) project for the validation and intercomparison of operational and semi-operational satellite rainfall estimates over Australia, USA and Europe in near real time (Ebert 2004; Janowiak et al. 2004; Kidd 2004). Whereas during warm months relatively deep convection may be a major contributor to precipitation amounts over the continental mid-latitudes, cold season precipitation is often less intense and more stratiform, and therefore it does not present a reliable microwave or infrared signature. The validation results of several international activities suggest that current satellite infrared rainfall estimation schemes are most likely to be useful in estimating climatic scale distributions of principally connective rainfall,

as is found in the warm season over mid-latitude continental interiors (Petty and Krajewski 1996). For wintertime conditions characterized by reduced convection and a greater percentage of shallow, fast-moving, less intense rainfall events, the infrared cloud top temperature is poorly correlated with the surface rainfall rate and produces a greater percentage of false alarms (i.e., higher bias) in the qualitative-type infrared estimates (Turk et al. 2006). Many studies have indicated the different performances of infrared-based techniques in warm or cold seasons in mid-latitudes over certain areas (Barrett 1970; Barrett and Martin 1981; Adler et al. 1993; Xie and Arkin 1995; Vicente and Scofield 1997; Smith et al. 1998; Vicente et al. 1998; Levizzani et al. 2002). The results of our study agree with the previous findings.

Comparison tests conducted in the different climate zones of the study area indicated that the calibrated CST performs better in the subtropical deserts and steppes of the northern Africa throughout the year, but with high relative errors, and in the humid continental climates for the three seasons of the year: summer, spring and winter. Mediterranean climates give higher correlations for autumn, summer and spring precipitation whereas humid sub-tropical climates present the lowest correlation coefficients, with the exception of summer precipitation.

The potential of the CST technique in climatic studies has been demonstrated by studying the diurnal variation of precipitation for the period May–August 2005 over the Greek Peninsula at high spatial and temporal resolutions. Data from rain gauges over Greece were used to verify the diurnal cycle derived by the CST estimates. Time series indicate a typical diurnal variation in precipitation with a pronounced rainfall maximum at between about 1400 and 1600 UTC (1700–1900 local time), which may be attributed to daytime heating. The timing of the diurnal cycle of the satellite estimates for both total rainfall and the division into convective and stratiform components was generally consistent with the analysis of rain gauge data. CST/Met-7 reproduced efficiently the convective component of precipitation. In examining just the stratiform component of rainfall, it was found that satellite estimates overestimate the rain gauge data. The calibrated CST overestimated slightly the

convective rainfall area but it provided an efficient division between convective and stratiform rain.

In summary, the infrared-based estimation technique presented can be used to reproduce the spatial distribution of accumulated precipitation in the Mediterranean region, but only for the warm season of the year. The same technique showed enough potential to be usable in obtaining the diurnal cycle of precipitation for the period and the area tested in this study.

Acknowledgements

References

Adler RF, Negri AJ (1988) A satellite infrared technique to estimate tropical convective and stratiform rainfall. J Appl Meteor 27: 30–51

Adler RF, Negri AJ, Keehn PR, Hakkarinen IM (1993) Estimation of monthly rainfall over Japan and surrounding waters from combination of low-orbit microwave and geosynchronous IR data. J Appl Meteor 32: 335–356

Arkin PA (1979) The relationship between fractional coverage of high clouds and rainfall accumulation during GATE over B-scale array. Mon Wea Rev 107: 1382–1387

Arkin PA, Meisner BN (1987) The relationship between large-scale convective rainfall and cold cloud over the western hemisphere during 1982–1984. Mon Wea Rev 115: 51–74

Arkin PA, Janowiak J (1991) Analysis of the global distribution of precipitation. Dyn Atmos Oceans 16: 5–16

Atlas D, Ulbrich CW, Marks FD Jr (2002) Reply to comment by Yuter SE, Houze RA Jr, on "Partitioning tropical oceanic convective and stratiform rains by draft strength" by Atlas D, et al. J Geophys Res 107(D1): 4006

Barrett EC (1970) The estimation of monthly rainfall from satellite data. Mon Wea Rev 98: 322–327

Barrett EC, Martin DW (1981) The use of satellite data for rainfall monitoring. Academic Press, London, 340 pp

Doneauld AA, Ionesku-Niscov S, Priegnitz DL, Smith PL (1984) The area time integral as an indicator for convective rain volume. J Climate Appl Meteor 23: 555–561

Ebert E, Manton M (1998) Performance of satellite rainfall estimation algorithms during TOGA COARE. J Atmos Sci 55: 1537–1557

Ebert E (2004) Monitoring the quality of operational and semi-operational satellite precipitation estimates – the IPWG validation/intercomparison study. 2nd IPWG Workshop, October 2004, Monterey, USA

Feidas H (2006) Validating three infrared-based rainfall retrieval algorithms for intense convective activity over Greece. Int J Remote Sensing 27: 2787–2812

Feidas H, Kokolatos G, Negri A, Manyin M, Chrysoulakis N (2006) A TRMM-calibrated infrared technique for rainfall estimation: application on rain events over eastern Mediterranean. Adv Geosci 7: 181–188

Goodison B, Louie P, Yang D (1998) WMO Solid Precipitation Measurement Intercomparison, Final Report. WMO/TD-No. 872, Instruments and Observing Methods No. 67, Geneva 1998, 88 pp

Griffith CG, Woodley WL, Browner S, Teijeiro J, Maier M, Martin DW, Stout J, Sikdar DN (1976) Rainfall estimation from geosynchronous satellite imagery during daylight hours. NOAA Technical Report ERC 356-WMPO 7, Washington, DC, USA

Griffith CG, Grube PG, Martin DW, Stout J, Sikdar DN (1978) Rainfall estimation from geosynchronous satellite imagery, visible and infrared studies. Mon Wea Rev 106: 1153–1171

Griffith CG, Augustine JA, Woodley WL (1981) Satellite rain estimation in the US high plains. J Appl Meteor 20: 53–66

Hong Y, Hsu K, Sorooshian S, Gao X (2004) Precipitation estimation from remotely sensed imagery using an artificial neural network cloud classification system. J Appl Meteor 43: 1834–1852

Hsu K, Gao X, Sorooshian S, Gupta HV (1997) Precipitation estimation from remotely sensed imagery using an artificial neural network. J Appl Meteor 36: 1176–1190

Janowiak JE (1992) Tropical rainfall: a comparison of satellite-derived rainfall estimates with model precipitation forecasts, climatologies and observations. Mon Wea Rev 120: 448–462

Janowiak JE, Xie P, Joyce RJ, Chen M, Yarosh Y (2004) Validation of satellite-derived rainfall estimates and numerical model forecasts of precipitation over United States. 2nd IPWG Workshop, October 2004, Monterey, USA

Joyce R, Janowiak J, Huffman G (2001) Latitudinally and seasonally dependent Zenith-angle corrections for geostationary satellite IR brightness temperatures. J Appl Meteor 40(4): 689–703

Kästner M (2003) Inter-comparison of precipitation estimations using TRMM microwave data and independent data. 3rd GPM Workshop, June 2003, ESTEC, Noordwijk, The Netherlands, pp 24–26

Kästner M, Torricella F, Davolio S (2006) Intercomparison of satellite-based and model-based rainfall analyses. Meteorol Appl 13: 213–223

Kidd C (2004) Validation of satellite rainfall estimates over the mid-latitudes. 2nd IPWG Workshop, October 2004, Monterey, USA

King PWS, Hogg WD, Arkin PA (1995) The role of visible data in improving satellite rain-rate estimates. J Appl Meteor 34: 1608–1621

Köppen W, Geiger R (1936) Das geographische System der Klimate. In: Köppen W, Geiger R (eds) Handbuch der Klimatologie. Bd 1, Teil C. Verlag Gebrüder Bornträger, Berlin (DE) (in German)

Legates DR (1987) A climatology of global precipitation. Publ. in Climatology, vol 40 (1), Newark, DW, 85 pp

Levizzani V, Porcu F, Prodi F (1990) Operational rainfall estimation using METEOSAT infrared imagery: an application in Italy's Arno River basin. Its potential and drawbacks. ESA Journal 14: 313–323

Levizzani V, Amorati R, Meneguzzo F (2002) A review of satellite-based rainfall estimation methods. MUSIC. www.isao.bo.cnr.it/meteosat/papers/MUSIC-Rep-Sat-Precip-6.1.pdf

Lopez RE, Atlas D, Rosenfeld D, Thomas JL, Blanchard DO, Holle RL (1989) Estimation of rainfall using the radar echo area time integral. J Appl Meteor 28: 1162–1175

Marrocu M, Pompei A, Dalu G, Liberti GL, Negri A (1993) Precipitation estimation over Sardinia from satellite infrared data. Int J Remote Sensing 14: 115–134

Menz G (1997) Regionalization of precipitation models in east Africa using Meteosat data. Int J Climatol 17: 1011–1027

Negri AJ, Adler RF, Wetzel PJ (1984) Satellite rain estimation: an analysis of the Griffith-Woodley technique. J Climate Appl Meteor 23: 102–116

Negri AJ, Adler RF, Xu L (2002) A TRMM calibrated rainfall algorithm applied over Brazil. J Geophys Res 107: 8048–8062

Negri AJ, Adler RF, Xu L (2003) A TRMM-calibrated infrared technique for global rainfall estimation. In: Proc. 12th Conf. Satellite Meteorology and Oceanography, February 2003, Long Beach, CA, USA, pp 9–13

Nzeukou A, Sauvageot H, Ochou AD, Kebe MF (2002) Raindrop size distribution and radar parameters at Cape Verde. J Appl Meteor 42: 1031–1034

Oh HJ, Sohn BJ, Smith EA, Turk FJ, Ae-Suk S, Chung HS (2002) Validating infrared-based rainfall retrieval algorithms with 1-minute spatially dense raingauge measurements over Korean peninsula. Meteorol Atmos Phys 81: 273–287

Petty GW, Krajewski WF (1996) Satellite estimation of precipitation over land. Hydrolog Sci 41(4): 433–451

Rudolf B, Schneider U (2005) Calculation of gridded precipitation data for the global land surface using in-situ gauge-observations. 2nd Workshop of the International Precipitation Working Group, Monterey, October 2004, USA

Schumacher C, Houze RA Jr (2003) Stratiform rain in the tropics as seen by the TRMM precipitation radar. J Climate 16: 1739–1756

Shepard D (1968) A two-dimensional interpolation function for irregularly spaced data. Proc. 23rd ACM Nat. Conf., Brandon/Systems Press, Princeton, NJ, pp 517–524

Smith EA, Lamm JE, Adler R, Alishouse J, Aonashi K, Barrett E, Bauer P, Berg W, Chang A, Ferraro R, Ferriday J, Goodman S, Grody N, Kidd C, Kniveton D, Kummerow C, Liu G, Marzano F, Mugnai A, Olson W, Petty G, Shibata A, Spencer R, Wentz F, Wilheit T, Zipser E (1998) Results of WetNet PIP-2 project. J Atmos Sci 55: 1483–1536

Tarruella R, Jorge J (2003) Comparison of three infrared satellite techniques to estimate accumulated rainfall over the Iberian Peninsula. Int J Climatol 23: 1757–1769

Tenório RS, Kwon B-H (2006) Z-R relationship and a severe rainfall observed by C-band radar in eastern coast of northeastern Brazil. In: Proc. 4th European Conference on Radar in Meteorology and Hydrology. ERAD, Barcelona, September 2006, pp 18–22

Turk FJ, Monterey NRL, Bauer CAP, Ebert E, Arkin PA (2006) Satellite-derived precipitation verification activities within the International Precipitation Working Group (IPWG). 14th Conference on Satellite Meteorology and Oceanography, 29 January–3 February 2006, Atlanta, GA, Lindsey

Vicente GA, Scofield RA, Menzel WP (1998) The operational GOES infrared rainfall estimation technique. Bull Amer Meteor Soc 79: 1883–1898

Willmott CJ, Rowe CM, Philpot WD (1985) Small-scale climate maps: a sensitivity analysis of some common assumptions associated with grid-point interpolation and contouring. Amer Cartogr 12: 5–16

WMO (1985) Review of requirements for area-averaged precipitation data, surface based and space based estimation techniques, space and time sampling, accuracy and error, data exchange. WCP-100, WMO/TD-No. 115

Xie P, Arkin PA (1995) An intercomparison of gauge observations and satellite estimates of monthly precipitation. J Appl Meteor 34(5): 1143–1160